A coupled periodic FE-BE model for ground-borne vibrations from underground railways

Shashank Gupta, Geert Degrande, Hamid Chebli, Didier Clouteau,
Mohammed F.M. Hussein, Hem Hunt

III European Conference on Computational Mechanics
Solids, Structures and Coupled Problems in Engineering
C.A. Mota Soares et.al. (eds.)
Lisbon, Portugal, 5–9 June 2006

A COUPLED PERIODIC FE-BE MODEL FOR GROUND-BORNE VIBRATIONS FROM UNDERGROUND RAILWAYS

S. Gupta[1], G. Degrande[1], H. Chebli[2], D. Clouteau[2], M.F.M. Hussein[3] and H. Hunt[3]

[1]Department of Civil Engineering, K.U. Leuven
B-3001 Leuven, Belgium
e-mail: shashank.gupta@bwk.kuleuven.be

[2] LMSSMat, Ecole Centrale de Paris
F-92295 Châtenay-Malabry, France
e-mail: clouteau@mss.ecp.fr

[3] Department of Engineering, University of Cambridge,
Cambridge CB2 1PZ, United Kingdom
e-mail: mfmh2@cam.ac.uk

Keywords: Periodic FE-BE method, ground vibration, dynamic track-tunnel-soil interaction, wheel and rail roughness, moving loads.

Abstract. *An efficient and modular numerical prediction model is presented to predict vibrations in the free field due to metro trains in the tunnel. The three-dimensional dynamic tunnel-soil interaction problem is solved with a subdomain formulation, using a finite element formulation for the tunnel and a boundary element method for the soil. The periodicity of the tunnel and the soil in the longitudinal direction is exploited using the Floquet transform, limiting the discretization effort to a single bounded reference cell. The Craig-Bampton substructuring technique is used to efficiently incorporate a track in the tunnel. The track-tunnel-soil interaction problem is solved in the frequency-wavenumber domain and the wave field radiated into the soil is computed.*

The numerical model can also account for moving loads and various excitation mechanisms, including quasi-static loads, random loads due to the rail and wheel unevenness, impact excitation due to the rail joints and wheel flats, and parametric excitation excitation due to the sleeper periodicity. In this paper, only the excitation due to rail unevenness and a moving harmonic load are considered. A general analytical formulation is discussed to compute the response of three-dimensional invariant and periodic media that are excited by moving loads.

To demonstrate the efficiency of the approach, an invariant tunnel with a concrete lining, embedded in a homogeneous full space is considered. The system is excited by a vehicle moving on an uneven rail. The free field vibrations are predicted, by first computing the contact forces generated by the wheel-track interaction and then solving the dynamic track-tunnel-soil interaction problem.

1 INTRODUCTION

Vibrations induced by underground railways are of a major environmental concern in urban areas. The study of these vibrations require three-dimensional models that account for the dynamic interaction between the track, the tunnel and the soil. Three-dimensional numerical models are developed by some researchers to model vibration from underground railways [1, 2, 3]. As three dimensional finite element models become prohibitively large, a boundary element formulation [4] is often preferred to model the soil as a horizontally layered medium. An excellent review of the boundary element technology applied to the dynamic analysis of three-dimensional underground structures is available [5, 6]. The main disadvantage of these models is that they are computationally expensive. This has been the main motivation to exploit the longitudinal invariance or periodicity of the track-tunnel-soil system. The Floquet transformation allows to limit the computational effort to a single bounded reference cell. This paradigm has been used for the study of the dynamic response of structures subjected to three-dimensional seismic loading [7].

In the coupled periodic finite element-boundary element (FE-BE) model, the three-dimensional dynamic tunnel-soil interaction problem is solved with a subdomain formulation, using a finite element method for the tunnel and boundary elements method for the soil, modelled as a horizontally layered elastic half space. The problem is formulated in the frequency-wavenumber domain on a reference cell using the Floquet transformation. The Craig-Bampton substructuring technique [8] is used to model a track in the tunnel. The numerical model is also capable of dealing with various types of moving loads, including quasi-static loads, random loads due to rail and wheel unevenness, impact excitation due to rail joints and wheel flats, and parametric excitation due to sleeper periodicity. A general analytical formulation is used to compute the response of three-dimensional invariant and periodic media that are excited by moving loads. The advantage of the approach is that the response is directly deduced from the transfer functions in the frequency-wavenumber domain calculated in the generic cell.

To demonstrate the efficiency of the approach, an invariant concrete tunnel embedded in a homogeneous full space is modelled as a periodic structure. The track is modelled as an infinite double beam on an elastic foundation and is coupled to the tunnel via a uniform support. The transfer functions of the track-tunnel-soil system have been validated with the semi-analytical solution, which is available from a so-called pipe-in-pipe model [9, 10, 11]. In the present paper, the same example is dealt with for the case of the excitation due to a moving harmonic load and the unevenness excitation due to rail roughness. After a short overview of the model, numerical results are presented.

2 COUPLED PERIODIC FE-BE MODEL

The coupled periodic FE-BE model is an effective prediction tool that accounts for the complex periodic geometry of the tunnel and the layering of a semi-infinite soil medium. A finite element method is used to model a tunnel reference cell, while a boundary element method is used to model the soil, as a horizontally layered elastic half space.

2.1 Floquet transform

An infinite periodic structure can be analyzed using the Floquet transform method. If the spatial period is L, then the position $\mathbf{x}$ of any point in the problem domain Ω is decomposed as $\mathbf{x} = \tilde{\mathbf{x}} + nL\mathbf{e}_y$, where $\tilde{\mathbf{x}}$ is the position in the reference cell $\tilde{\Omega}$ and n is the cell number. The Floquet transformation $\tilde{f}(\tilde{\mathbf{x}}, \kappa)$ of a non-periodic function $f(\mathbf{x}) = f(\tilde{\mathbf{x}} + nL\mathbf{e}_y)$ defined on a

domain Ω, that is periodic in the direction $\mathbf{e}_y$ with period L, transforms the distance nL between the n-th cell and the reference cell $\tilde{\Omega}$ to the wave number $\kappa \in [-\pi/L, \pi/L]$ and is defined as [7]:

$$\tilde{f}(\tilde{\mathbf{x}}, \kappa) = \sum_{n=-\infty}^{+\infty} f(\tilde{\mathbf{x}} + nL\mathbf{e}_y) \exp(+inL\kappa) \tag{1}$$

The complex valued function $\tilde{f}(\tilde{\mathbf{x}}, \kappa)$ is a periodic function of κ with a period $2\pi/L$ (or a periodic function of the first kind with respect to κ), as the following periodicity condition holds:

$$\tilde{f}(\tilde{\mathbf{x}}, \kappa + \frac{2\pi}{L}) = \tilde{f}(\tilde{\mathbf{x}}, \kappa) \tag{2}$$

This complex function $\tilde{f}(\tilde{\mathbf{x}}, \kappa)$ is also periodic of the second kind with a period L in the direction $\mathbf{e}_y$ since the following condition holds for all $\tilde{\mathbf{x}}$:

$$\tilde{f}(\tilde{\mathbf{x}} + L\mathbf{e}_y, \kappa) = \exp(-i\kappa L)\tilde{f}(\tilde{\mathbf{x}}, \kappa) \tag{3}$$

The inverse Floquet transform is defined as:

$$f(\tilde{\mathbf{x}} + nL\mathbf{e}_y) = \frac{L}{2\pi} \int_{-\pi/L}^{+\pi/L} \tilde{f}(\tilde{\mathbf{x}}, \kappa) \exp(-inL\kappa) \mathrm{d}\kappa \tag{4}$$

This definition will be used to synthesize the solution on the problem domain Ω if it is known on the reference cell $\tilde{\Omega}$.

2.2 Dynamic tunnel-soil

The numerical solution of the dynamic tunnel-soil interaction problem is obtained using the classical domain decomposition approach based on the finite element method for the tunnel and the boundary element method for the soil.

As the tunnel is bounded, the displacement field $\tilde{\mathbf{u}}_t(\tilde{\mathbf{x}}, \kappa, \omega)$ in the tunnel can be decomposed on a basis of functions $\tilde{\psi}_m(\tilde{\mathbf{x}}, \kappa)$:

$$\tilde{\mathbf{u}}_t(\tilde{\mathbf{x}}, \kappa, \omega) = \sum_{m=1}^{N} \tilde{\psi}_m(\tilde{\mathbf{x}}, \kappa) \alpha_m(\kappa, \omega) \tag{5}$$

where $\tilde{\psi}_m(\tilde{\mathbf{x}}, \kappa)$ is the kinematical basis that obeys the periodicity condition of the second kind (equation (3)).

The soil displacements $\tilde{\mathbf{u}}_s(\tilde{\mathbf{x}}, \kappa, \omega)$ can be written as the superposition of waves that are radiated by the tunnel into the soil:

$$\tilde{\mathbf{u}}_s(\tilde{\mathbf{x}}, \kappa, \omega) = \tilde{\mathbf{u}}_{\mathrm{sc}}(\tilde{\mathbf{u}}_t)(\tilde{\mathbf{x}}, \kappa, \omega) = \sum_{m=1}^{M} \tilde{\mathbf{u}}_{\mathrm{sc}}(\tilde{\psi}_m)(\tilde{\mathbf{x}}, \kappa, \omega) \alpha_m(\kappa, \omega) \tag{6}$$

The weak or variational formulation of the problem results in the following system of equations in the frequency-wavenumber domain: [7, 12, 13, 14]:

$$\left[\mathbf{K}_t(\kappa) - \omega^2 \mathbf{M}_t(\kappa) + \mathbf{K}_s(\kappa, \omega)\right] \alpha(\kappa, \omega) = \mathbf{F}_t(\kappa, \omega) \tag{7}$$

where $\mathbf{K}_t(\kappa)$ and $\mathbf{M}_t(\kappa)$ are the projection of the finite element stiffness matrix and mass matrix of the tunnel reference cell on the tunnel modes $\tilde{\psi}_m(\tilde{\mathbf{x}}, \kappa)$ (which are periodic of the second kind). $\mathbf{K}_s(\kappa, \omega)$ is the dynamic stiffness matrix of the soil calculated with a periodic boundary element formulation with Green-Floquet functions defined on the periodic structure with period L along the tunnel [7, 12, 13, 15].

The Craig-Bampton substructuring technique is used to efficiently incorporate a track in the tunnel, describing the kinematics of the track-tunnel system as a superposition of the track modes on a rigid base and the quasi-static transmission of the free tunnel modes into the track. The advantage of this approach is that the soil impedance only depends on the periodic tunnel modes and does not change when alternative track structures are considered.

Equation (7) is solved to obtain the displacement field in the reference cell in the frequency-wavenumber domain. When the displacements $\tilde{\mathbf{u}}_t(\tilde{\mathbf{x}}, \kappa, \omega)$ and the stresses $\tilde{\mathbf{t}}_t(\tilde{\mathbf{x}}, \kappa, \omega)$ on the tunnel-soil interface are known, the wave field radiated into the soil is computed using the dynamic representation theorem in the unbounded soil domain corresponding to the reference cell. The displacement field in the frequency domain at any point $\mathbf{x}$ in another cell is obtained after evaluation of the inverse Floquet transform (equation (4)).

3 THE RESPONSE DUE TO MOVING LOADS

In the fixed frame of reference, the distribution of n vertical axle loads on the coupled track-tunnel-soil system is written as the summation of the product of Dirac functions that determine the time-dependent position $\mathbf{x}^S = \{x^S, y_k + vt, z^S\}^{\mathrm{T}}$ and the time history $g_k(t)$ of the k-th axle load:

$$\mathbf{F}(\mathbf{x}, t) = \sum_{k=1}^{n} \delta(x - x^S)\delta(y - y_k - vt)\delta(z - z^S) g_k(t) \mathbf{e}_z \tag{8}$$

y_k is the initial position of the k-th axle that moves with the train speed v along the y-axis and $\mathbf{e}_z$ denotes the vertical unit vector.

A Fourier transformation is applied to equation (8) to obtain the representation in the frequency-spatial domain:

$$\hat{\mathbf{F}}(\mathbf{x}, \omega) = \frac{1}{v} \sum_{k=1}^{n} g_k(\frac{y - y_k}{v}) \exp\left[- i\frac{\omega}{v}(y - y_k)\right] \delta(x - x^S)\delta(z - z^S)\mathbf{e}_z \tag{9}$$

The response in the frequency domain $\hat{u}_i(\mathbf{x}, \omega)$ at the receiver point $\mathbf{x}$ due to k-th axle load is written as the superposition of the load distribution along the source line:

$$\hat{u}_i(\mathbf{x}, \omega) = \int_{-\infty}^{\infty} \hat{F}_{kz}(\mathbf{x}', \omega) \hat{h}_{zi}(\mathbf{x}', \mathbf{x}, \omega) \mathrm{d}y' \tag{10}$$

where $\hat{F}_{kz}$ is the vertical component of the k-th axle load and $\hat{h}_{zi}(\mathbf{x}', \mathbf{x}, \omega)$ is the transfer function, expressing the displacement at $\mathbf{x}$ in the $\mathbf{e}_i$ direction, due to a unit load applied at $\mathbf{x}'$ in the $\mathbf{e}_z$ direction. Substituting equation (9) in equation (10) and omitting the dependance on the source coordinates x' and z' gives:

$$\hat{u}_i(\mathbf{x}, \omega) = \frac{1}{v} \int_{-\infty}^{\infty} g_k(\frac{y' - y_k}{v}) \exp\left[- i\frac{\omega}{v}(y' - y_k)\right] \hat{h}_{zi}(y', \mathbf{x}, \omega) \mathrm{d}y' \tag{11}$$

$$= \int_{-\infty}^{\infty} g_k(\tau) \hat{h}_{zi}(y_k + v\tau, \mathbf{x}, \omega) \exp\left(-i\omega\tau\right) \mathrm{d}\tau \tag{12}$$

The response due to a moving load on the track can therefore be calculated from the receptance of the track-tunnel-soil system describing the displacement at a point $\mathbf{x}$ due to a load at position $\mathbf{x}'$. In case of an invariant or a periodic geometry, the expressions (11) and (12) can be further simplified.

3.1 Invariant domains

In the case of invariant geometries, the transfer function $\hat{h}_{zi}$ only depends on the relative position between the source and the receiver:

$$\hat{u}_i(\mathbf{x},\omega) = \int_{-\infty}^{\infty} g_k(\tau)\hat{h}_{zi}(x, y-y_k-v\tau, z, \omega)\exp\left(-i\omega\tau\right)\mathrm{d}\tau \tag{13}$$

The Fourier transformation of the longitudinal coordinate y to the wavenumber k_y gives the response in the frequency-wavenumber domain:

$$\tilde{u}_i(x,k_y,z,\omega) = \hat{g}_k(\omega-k_y v)\tilde{h}_{zi}(x,k_y,z,\omega)\exp\left(ik_y y_k\right) \tag{14}$$

The frequency shift $k_y v$ between the circular frequency at the receiver and at the source corresponds to the Doppler effect. The response in the space-frequency domain is obtained as the inverse Fourier transform of equation (14):

$$\hat{u}_i(\mathbf{x},\omega) = \frac{1}{2\pi}\int_{-\infty}^{\infty}\hat{g}_k(\omega-k_y v)\tilde{h}_{zi}(x,k_y,z,\omega)\exp\left[-ik_y(y-y_k)\right]\mathrm{d}k_y \tag{15}$$

$$= \frac{1}{2\pi v}\int_{-\infty}^{\infty}\hat{g}_k(\tilde{\omega})\tilde{h}_{zi}(x,\frac{\omega-\tilde{\omega}}{v},z,\omega)\exp\left[-i(\frac{\omega-\tilde{\omega}}{v})(y-y_k)\right]\mathrm{d}\tilde{\omega} \tag{16}$$

where $k_y = (\omega-\tilde{\omega})/v$. Compared to equation (13), this approach offers the advantage that the transfer function is evaluated in the frequency-wavenumber domain. This approach was developed and used by Lombaert [16] for the prediction of free field vibrations induced by road traffic.

3.2 Periodic domains

A periodic geometry has a spatial period L and it is assumed that the receiver point is in the generic cell $\mathbf{x} = \tilde{\mathbf{x}}$. The axle load $g_k((y'-y_k)/v)$ in equation (11) is expressed in terms of its Fourier transform, so that the response becomes:

$$\hat{u}_i(\tilde{\mathbf{x}},\omega) = \frac{1}{2\pi v}\int_{-\infty}^{\infty}\int_{-\infty}^{\infty}\hat{g}_k(\tilde{\omega})\exp\left[-i\frac{\omega-\tilde{\omega}}{v}(y'-y_k)\right]\hat{h}_{zi}(y',\tilde{\mathbf{x}},\omega)\mathrm{d}y'\,\mathrm{d}\tilde{\omega} \tag{17}$$

Substituting $y' = \tilde{y}' + nL$ gives:

$$\hat{u}_i(\tilde{\mathbf{x}},\omega) = \frac{1}{2\pi v}\int_{-\infty}^{\infty}\hat{g}_k(\tilde{\omega})\int_{-L/2}^{L/2}\sum_{n=-\infty}^{\infty}\exp\left[-i\frac{\omega-\tilde{\omega}}{v}(\tilde{y}'+nL-y_k)\right]$$
$$\times\ \hat{h}_{zi}(\tilde{y}'+nL,\tilde{\mathbf{x}},\omega)\,\mathrm{d}\tilde{y}'\,\mathrm{d}\tilde{\omega} \tag{18}$$

Due to the geometric periodicity, the following equation holds:

$$\hat{h}_{zi}(\tilde{y}'+nL,\tilde{\mathbf{x}},\omega) = \hat{h}_{zi}(\tilde{y}',\tilde{\mathbf{x}}-nL\mathbf{e}_y,\omega) \tag{19}$$

From equations (18) and (19) and the definition of the Floquet transform (1), the following expression is obtained:

$$\begin{aligned}\hat{u}_i(\tilde{\mathbf{x}},\omega) &= \frac{1}{2\pi v}\int_{-\infty}^{\infty}\hat{g}_k(\tilde{\omega})\exp\left[i(\frac{\omega-\tilde{\omega}}{v})y_k\right] \\ &\times \int_{-L/2}^{L/2}\exp\left[-i(\frac{\omega-\tilde{\omega}}{v})\tilde{y}'\right]\tilde{\hat{h}}_{zi}(\tilde{y}',\tilde{\mathbf{x}},\kappa_0,\omega)\,\mathrm{d}\tilde{y}'\,\mathrm{d}\tilde{\omega}\end{aligned} \tag{20}$$

where $\kappa_0 = \frac{\omega-\tilde{\omega}}{v} - \frac{2m\pi}{L}$ with $\kappa_0 \in]-\pi/L, \pi/L[$ and m is an integer. $\tilde{\hat{h}}_{zi}(\tilde{y}',\tilde{\mathbf{x}},\kappa_0,\omega)$ is the Floquet transform of the transfer function $\hat{h}_{zi}(\tilde{y}',\tilde{\mathbf{x}}+nL\mathbf{e}_y,\omega)$. The response at another point $\mathbf{x}=\tilde{\mathbf{x}}+nL\mathbf{e}_y$ is obtained using the periodicity of the second kind (3) on the transfer function. Hence, the response in the periodic domain due to the k-th axle load $g_k(t)$ is given by:

$$\begin{aligned}\hat{u}_i(\tilde{\mathbf{x}}+nL\mathbf{e}_y,\omega) &= \frac{1}{2\pi v}\int_{-\infty}^{\infty}\hat{g}_k(\tilde{\omega})\exp\left[-i(\frac{\omega-\tilde{\omega}}{v})(nL-y_k)\right] \\ &\times \int_{-L/2}^{L/2}\exp\left[-i(\frac{\omega-\tilde{\omega}}{v})\tilde{y}'\right]\tilde{\hat{h}}_{zi}(\tilde{y}',\tilde{\mathbf{x}},\kappa_0,\omega)\,\mathrm{d}\tilde{y}'\,\mathrm{d}\tilde{\omega}\end{aligned} \tag{21}$$

A change of variables according to $k_y = (\omega-\tilde{\omega})/v$ yields:

$$\begin{aligned}\hat{u}_i(\tilde{\mathbf{x}}+nL\mathbf{e}_y,\omega) &= \frac{1}{2\pi}\int_{-\infty}^{\infty}\hat{g}_k(\omega-k_y v)\exp\left[-ik_y(nL-y_k)\right] \\ &\times \int_{-L/2}^{L/2}\exp\left[-ik_y\tilde{y}'\right]\tilde{\hat{h}}_{zi}(\tilde{y}',\tilde{\mathbf{x}},\kappa_0,\omega)\,\mathrm{d}\tilde{y}'\,\mathrm{d}k_y\end{aligned} \tag{22}$$

where $\kappa_0 = k_y - 2m\pi/L$.

Comparison of these results with the case of invariant domains (equations (15) and (16)) demonstrates that an additional integral over the cell has to be evaluated in order to obtain the response in periodic domains. The advantage of the present approach is that the response due to moving loads is directly deduced from the transfer functions in the frequency-wavenumber domain, calculated in the generic cell.

4 EXCITATION MODEL

Significant vibrations in buildings near railway tracks and subway tunnels are attributed to moving trains. The excitation models developed under CONVURT [17, 18] account for three excitation mechanisms: the unevenness excitation due to wheel and rail roughness, the impact excitation due to rail joints and wheel flats, and the parametric excitation due to sleeper periodicity. In this paper, only forces due to rail roughness are considered.

Roughness is probably the main excitation source in the generation of vibrations from moving trains. According to the Remington's theory [19], undulations in the surface profile of both wheel and rail introduce relative motion between wheel and rail that excite the wheel-rail system. In Remington's model, the surface unevenness is described by a spectrum giving the r.m.s roughness level $u_{w/r}$ (in dB) versus the wavelength. The resolution is carried out in the frequency domain using the relation $f = v/\lambda_y$, where f is the excitation frequency, v is the speed and λ_y is the roughness wavelength.

Alternatively, the rail roughness is expressed as a stochastic process characterized by a single-sided power spectral density (PSD) $\tilde{S}_{w/r}(k_y)$, written as a function of the wavenumber

$k_y = \omega/v = 2\pi/\lambda_y$ [20]:

$$\tilde{S}_{w/r}(k_y) \;=\; \tilde{S}_{w/r}(k_{y0}) \left(\frac{k_y}{k_{y0}}\right)^{-w} \tag{23}$$

The parameters $\tilde{S}_{w/r}(k_{y0})$ and w depend on the quality of the rail unevenness. For railway unevenness, $k_{y0} = 1$ rad/m and $w = 3.5$ are commonly assumed. The upper and lower bound of the rail unevenness are $\tilde{S}_{w/r}(k_{y0}) = 5.0 \times 10^{-7}\,\mathrm{m}^3/\mathrm{rad}$ and $\tilde{S}_{w/r}(k_{y0}) = 1.0 \times 10^{-9}\mathrm{m}^3/\mathrm{rad}$, respectively. An artificial profile is generated from the PSD-curve based on the superposition of simple random processes with known statistical properties. The PSD $\hat{S}_{w/r}(\omega)$ of the unevenness in the frequency domain is found as $1/v\tilde{S}_{w/r}(-\omega/v)$ and increases with the vehicle speed proportional to $v^{2.5}$, where $w = 3.5$ in equation (23). Thus, an increase in speed is expected to give rise to higher dynamic axle loads and higher vibration levels.

For a linear system which is not varying, the equation of motion can be expressed in the frequency domain. This cannot be done in the case of impact excitation, where the phenomenon is non-linear due to the separation between the wheel and the rail. The impact force calculations are then performed in the time domain. The simple case of vertical interaction between the wheel and the rail is considered. The contact force $\hat{g}(\omega)$ in the frequency domain, generated due to an uneven profile is given by [21]:

$$\hat{g}(\omega) \;=\; \frac{\hat{u}_{w/r}(\omega)}{\hat{C}^v(\omega) + \hat{C}^c(\omega) + \hat{C}^t(\omega)} \tag{24}$$

$\hat{u}_{w/r}(\omega)$ is the relative displacement (roughness) between the wheel and the rail, and $\hat{C}^v(\omega)$, $\hat{C}^c(\omega)$, $\hat{C}^t(\omega)$ are the compliance of the vehicle, the contact spring and the track, respectively.

The force deflection relation of the contact stiffness is assumed to follow the Hertz law and can be given in the form:

$$g \;=\; G_H(u_w - u_r - u_{w/r})^{3/2} \tag{25}$$

where g is the wheel-rail contact force, u_w and u_r are the wheel and rail displacement respectively, $u_{w/r}$ is the roughness and G_H is the Hertzian constant. This nonlinear equation can be linearized for small displacement relative to the quasi-static deflection, to give an approximate stiffness for the contact spring [21].

When the wave speed in the rail is much higher than the train speed, assuming that the wheel is stationary is an acceptable approximation. This has been used in the analysis here, as a low speed approximation to compute the track receptance for a static unit load applied on the rail.

4.1 Track receptance

The excitation model considers the track-bed as a rigid foundation, which is suitable for modelling of modern tracks where the stiffness of the slab bearings is much smaller than the stiffness of the track-bed. This approach can be used, for example, to model a floating slab track, which is an effective measure of vibration isolation in underground tunnels. Figure 1 shows a floating slab track, where rubber bearings (or steel springs) are accommodated between the slab and the tunnel bed.

The model consists of two infinite Euler beams, representing the (two) rails and the slab, respectively. The rail has a bending stiffness EI_r and a mass m_r per unit length, and the slab has a bending stiffness EI_{sl} and a mass m_{sl} per unit length. The rail pads are modelled with

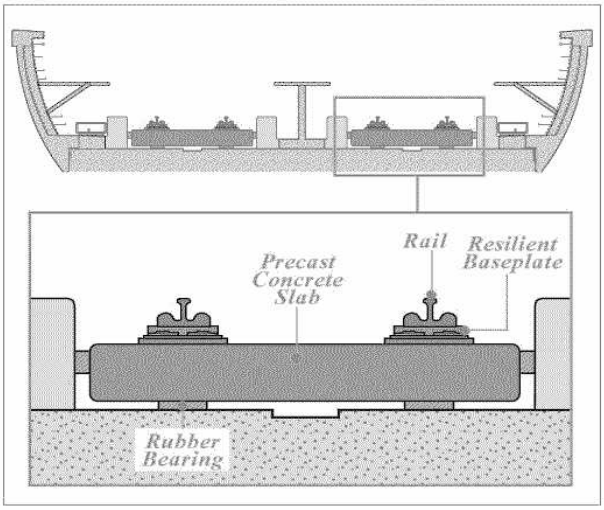

Figure 1: A floating-slab track: the concrete track slab is mounted on rubber bearings.

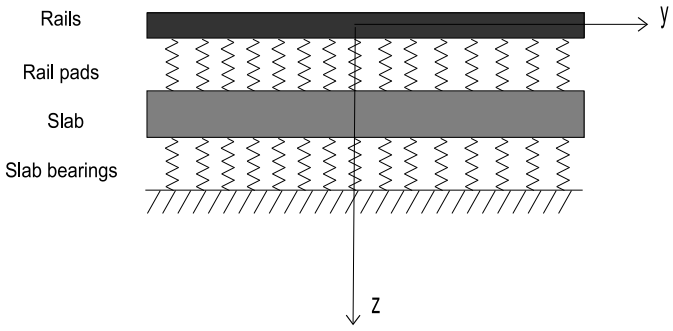

Figure 2: Infinite double beam on elastic foundation

a continuous support between both beams, while the subgrade is modelled with a continuous support below the lower beam (figure 2).

It is assumed in the following that the geometry of the track is invariant with respect to the longitudinal coordinate y. A Fourier transformation of the coordinate y to the wavenumber k_y can be performed to formulate the problem in the frequency-wavenumber domain. The equations of motion of the track can be written in a general form:

$$\begin{bmatrix} 2(\tilde{K}_r + \tilde{K}_{rp}) & -2\tilde{K}_{rp} \\ -2\tilde{K}_{rp} & \tilde{K}_{sl} + \tilde{K}_s + 2\tilde{K}_{rp} \end{bmatrix} \begin{Bmatrix} \tilde{u}_{rz} \\ \tilde{u}_{sz} \end{Bmatrix} = \begin{Bmatrix} 2\tilde{f}_r \\ 0 \end{Bmatrix} \tag{26}$$

where $\tilde{K}_r$ denotes the rail impedance $EI_r k_y^4 - m_r\omega^2$ in the frequency-wavenumber domain, and $\tilde{K}_{rp}$ is the dynamic stiffness $\bar{k}_{rp}(1 + i\eta_{rp})$ of the rail pads, with $\bar{k}_{rp}$ and η_{rp} the smeared stiffness and hysteretic damping factor of the rail pads, respectively. $\tilde{K}_{sl}$ is the slab impedance $EI_{sl}k_y^4 - m_{sl}\omega^2$, and $\tilde{K}_s$ is the dynamic stiffness $\bar{k}_s(1 + i\eta_s)$ of the slab bearings, with $\bar{k}_s$ and η_s the smeared stiffness and hysteretic damping factor of the slab bearings, respectively. $\tilde{f}_r$ is the force applied on a rail. The factor of two appears in the above equation to account for the two rails in the model. This modelling considers identical inputs on both rails. Equation (26)

is solved for the displacements of the rail $\tilde{u}_{rz}$ and the slab $\tilde{u}_{sz}$ in the frequency-wavenumber domain. The response in the frequency-spatial domain is obtained by evaluating the inverse Fourier transform with respect to wavenumber k_y:

$$\hat{u}_z(y,\omega) = \frac{1}{2\pi}\int_{-\infty}^{\infty} \tilde{u}_z(k_y,\omega)\exp\left(-ik_y y\right)\mathrm{d}k_y \tag{27}$$

The vertical point receptance of the rail is calculated for a unit impulse on both rails ($\tilde{f}_r$ = 1) as $\hat{C}^t(\omega) = \hat{u}_{rz}(0,\omega)$.

4.2 Wheel receptance

The wheel receptance depends on the intrinsic dynamic behavior of the wheel, but also on the axle bending modes and on the bogie and carriage suspension. Therefore, it is more judicious to use the rolling stock receptance at the contact point between the wheel and the rail.

The rolling stock receptance at the wheel-rail contact point is calculated using a transfer matrix method, relating the forces and displacements at the top of the rolling stock and at the contact point by the product of elementary transfer functions [18].

The rolling stock is decomposed into several subsystems (masses, springs and dampers), representing, for example, the mass of the wheel tread (M_1), the wheel web and axle per wheel (M_2), the bogie (M_3) and the carriage (M_4), as well as the stiffness of the resilient ring (K_1^*), the primary suspension (K_2) and the secondary suspension (K_3). Figure 3 shows this spring-mass-damper model. C_2 and C_3 are the viscous damping factors of the primary and the secondary suspensions.

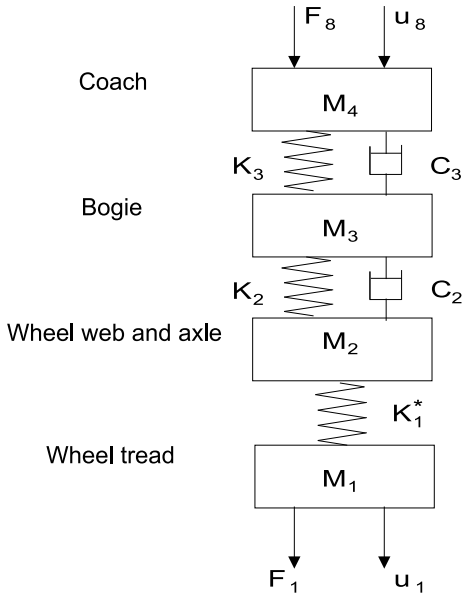

Figure 3: Rolling stock decomposition into subsystems

Each elementary sub-system is described by a 2 by 2 transfer matrix $\mathbf{T}$, which relates the displacements and forces at one end of the unit to the other end:

$$\left\{ \begin{array}{c} \hat{F}_{i+1} \\ \hat{u}_{i+1} \end{array} \right\} = \mathbf{T} \left\{ \begin{array}{c} \hat{F}_{i} \\ \hat{u}_{i} \end{array} \right\} \tag{28}$$

The subscript z is omitted here, though, the transfer matrix approach is limited to vertical displacements and forces. The corresponding transfer matrices for a mass M, a damped spring K^* and a spring-dashpot system characterized by K and C, are given as:

$$\begin{aligned} \mathbf{T}_M &= \begin{bmatrix} 1 & -M\omega^2 \\ 0 & 1 \end{bmatrix} \\ \mathbf{T}_{K^*} &= \begin{bmatrix} 1 & 0 \\ 1/K^* & 1 \end{bmatrix} \\ \mathbf{T}_{KC} &= \begin{bmatrix} 1 & 0 \\ 1/(K+i\omega C) & 1 \end{bmatrix} \end{aligned} \tag{29}$$

Thus, the forces and displacements at the top of the rolling stock and at the contact point are linked by the product of the elementary transfer matrices. For the subsystem decomposition shown in figure 3, the forces at the two ends of the system are related as:

$$\begin{Bmatrix} \hat{F}_8 \\ \hat{u}_8 \end{Bmatrix} = \mathbf{T}_{M_4}\mathbf{T}_{K_3C_3}\mathbf{T}_{M_3}\mathbf{T}_{K_2C_2}\mathbf{T}_{M_2}\mathbf{T}_{K_1^*}\mathbf{T}_{M_1} \begin{Bmatrix} \hat{F}_1 \\ \hat{u}_1 \end{Bmatrix} \tag{30}$$

The receptance at the contact point $\hat{C}^v = \hat{u}_1$ in the frequency domain, is obtained by setting $\hat{F}_8 = 0$ and $\hat{F}_1 = 1$.

The advantage of this methods is that it allows to include several complex subsystems with user-defined transfer matrices, obtained from finite element analysis or experiments. This allows, for example, to account for the effect of a flexible wheel-set in the rolling stock receptance.

5 Numerical example

To demonstrate the efficiency of the approach, an invariant tunnel embedded in homogeneous full space is considered. The transfer functions of the track-tunnel-soil system have been validated with the analytical solution of this problem, which is readily available from the pipe-in-pipe model [9, 10, 11]. Presently, the response due to moving harmonic load and a rolling stock moving on a rough rail are computed.

5.1 Problem outline

An invariant tunnel is considered, embedded in homogeneous soil that is modelled as a full space without the presence of a free surface. The invariant tunnel is idealized as a periodic system with a spatial period $L = 0.5$ m. The tunnel has an internal radius $r_i = 2.75$ m and a wall thickness $t = 0.25$ m. The tunnel has material properties of concrete: a Young's modulus $E^t = 50 \times 10^9$ Pa, a Poisson's ratio $\nu^t = 0.3$ and a density $\rho^t = 2500$ kg/m^3. The soil has a shear wave velocity $C_s = 309$ m/s, a longitudinal wave velocity $C_p = 944$ m/s, a density $\rho = 2000$ kg/m^3 and a hysteretic material damping ratio $\beta_s = \beta_p = 0.03$ in shear and volumetric deformation.

The track is modelled as an infinite double Euler-Bernoulli beam on an elastic foundation, where the upper beam represents the rails with bending stiffness $EI_r = 6.4 \times 10^6$ Nm^2 and mass per unit length $m_r = 60$ kg/m, and the lower beam represents the slab with bending stiffness $EI_{sl} = 1430 \times 10^6$ Nm^2 and mass per unit length $m_{sl} = 3500$ kg/m. A soft rail pad with stiffness $k_{rp} = 14.2$ MN/m and the vertical damping factor $\eta_{rp} = 0.5$ is considered in this example. This stiffness is smeared along the longitudinal direction of the track, accounting for the sleeper

distance $d = 0.6$ m. Thus, the vertical stiffness of the continuous support representing the rail pad is $\bar{k}_{rp} = k_{rp}/d = 23.68\,\text{MN/m}^2$. A soft rail pad is purposely chosen for the computations, to make the resonance of the rail on rail pads fall below 200 Hz, the maximum frequency which will be considered here. The floating slab tracks has an isolation frequency $f_{\text{iso}} = 20$ Hz. Hence, the stiffness per unit length of the subgrade is $\bar{k}_s = 55.27\,\text{MN/m}^2$. The loss factor $\eta_s = 0.5$ is used for damping in the subgrade under the slab.

5.2 Response to a non-moving harmonic load

The results are presented in the frequency range 1-200 Hz for the tunnel-soil interaction without the track and for the dynamic interaction including the track. The performance of the floating slab track as a vibration counter measure is assessed in the following.

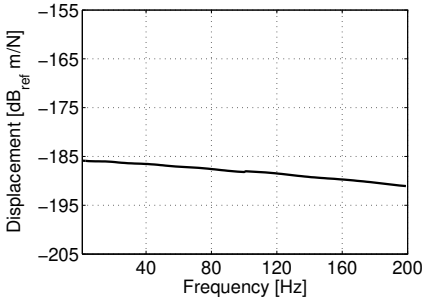

Figure 4: Vertical response at the tunnel invert due to a unit impulse applied at the tunnel invert for the case of the tunnel without the track.

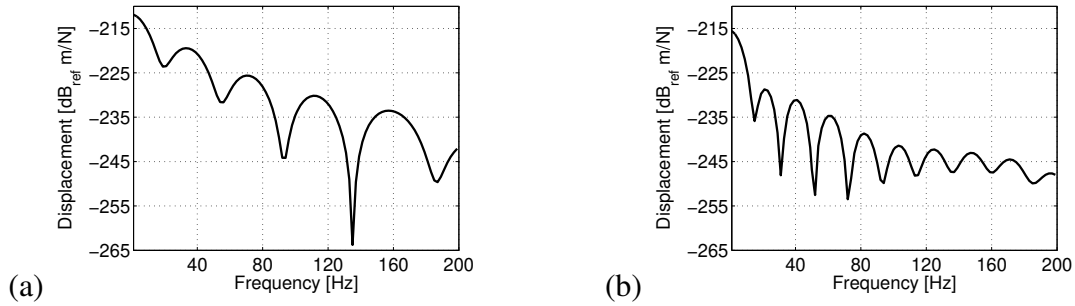

Figure 5: Vertical response at (a) 10 m and (b) 20 m above the tunnel due to a unit impulse applied at the tunnel invert for the case of the tunnel without the track.

Figure 4 shows the vertical transfer function at the tunnel invert for a unit impulse applied at the tunnel invert. The response does not exhibit any peak or resonance. The presence of soil as an infinite full space around the tunnel suppresses the resonance of the tunnel, as energy is dissipated due to the geometrical and material damping in the soil. Figure 5 shows the vertical response at 10 m and 20 m above the tunnel. The response is characterized by an undulating behavior giving rise to crests and troughs at constant frequency steps. This is due to the interference of the compression and shear waves at a particular distance from the source.

Next, the floating slab track is considered inside the tunnel. It is subjected to a symmetrical loading with $\tilde{f}_r = 0.5$ N on each rail and is equivalent to $2\tilde{f}_r = 1$ N load on the track-tunnel-soil system. Figure 6 compares the vertical response of the rail, computed from the track model

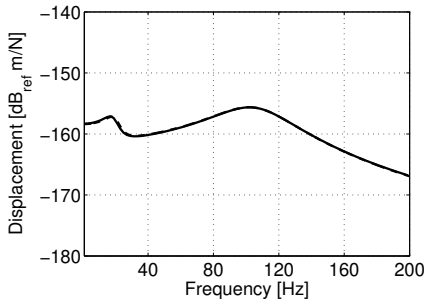

Figure 6: Vertical response of the rails for $\tilde{f}_r = 0.5$ N applied on each rail, computed with the track model on a rigid base (solid line) and with the coupled periodic FE-BE model accounting for dynamic track-tunnel-soil interaction (dashed line).

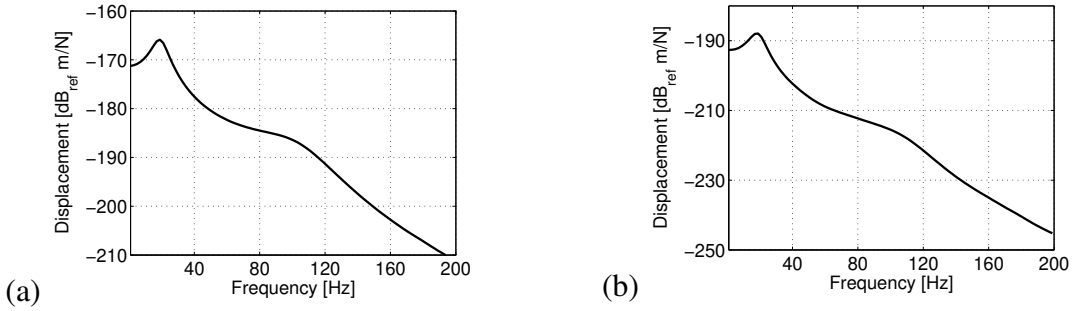

Figure 7: Vertical response at (a) the slab and (b) the tunnel invert due to the load $\tilde{f}_r = 0.5$ N applied on each rail.

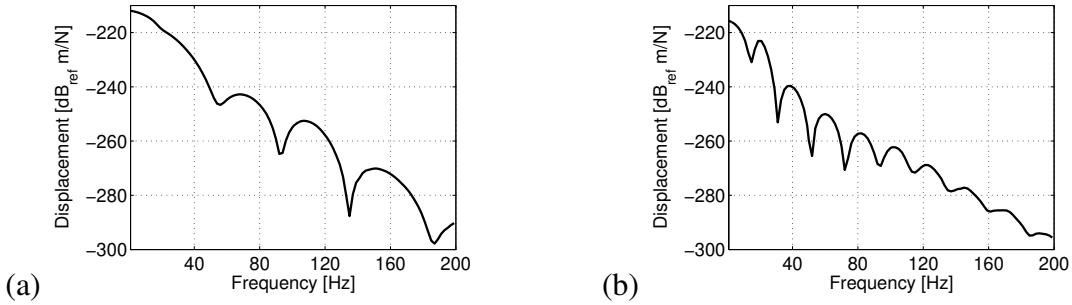

Figure 8: Vertical response at (a) 10 m and (b) 20 m above the tunnel due to the load $\tilde{f}_r = 0.5$ N applied on each rail.

consisting of two Euler-Bernoulli beams on a rigid base and from the coupled periodic FE-BE model accounting for the additional flexibility of the tunnel and supporting soil. The good agreement between the two cases justifies the assumption of using a rigid base model for the calculation of the interaction force due to rail and wheel unevenness (cfr. section 4). Two peaks appear in the response of the rail. The first peak appears at a value less than the isolation frequency of the slab, which corresponds to the uncoupling of the track on the stiffness of the subgrade. This frequency can be approximately calculated as $1/(2\pi)\sqrt{\bar{k}_s/(m_{sl}+2m_r)} = 19.66$ Hz. The second peak is the cut-on frequency, where the waves propagate only in the rail, while the slab does not move. Again, the value of the second cut-on frequency can be

approximately calculated using the mass per unit length m_r of the rail and the smeared stiffness of the rail pads $\bar{k}_{rp}$, as $1/(2\pi)\sqrt{\bar{k}_{rp}/m_r} = 100.00$ Hz.

Figure 7 shows the response at the slab and the tunnel invert, when the track is installed inside the tunnel. Unlike the response of the tunnel without the track, a resonance peak is observed at approximately the isolation frequency of the slab. Similarly, figure 8 shows the response at 10 m and 20 m above the tunnel. It can be observed that the response has reduced in the free field due to the installation of the floating slab. The energy propagates along the slab, before being transmitted to the tunnel and then soil.

A useful way to evaluate the effectiveness of the floating slab track is to take the ratio of the response with and without the resilient bearings inserted between the slab and tunnel invert. The concept of insertion gain in dB will be used, which indicates the increase in vibration levels caused by the bearings. The insertion gain is defined as the ratio of the response u^{iso} of the isolated and the response u^{uniso} of the unisolated system:

$$\text{IG [dB]} = 20 \log \left(\frac{u^{\text{iso}}}{u^{\text{uniso}}} \right) \tag{31}$$

Figure 9 shows the insertion gain at 10 m and 20 m above the tunnel. For a 20 Hz floating slab track, the insertion gain becomes negative at frequencies greater than 27 Hz, indicating the isolation.

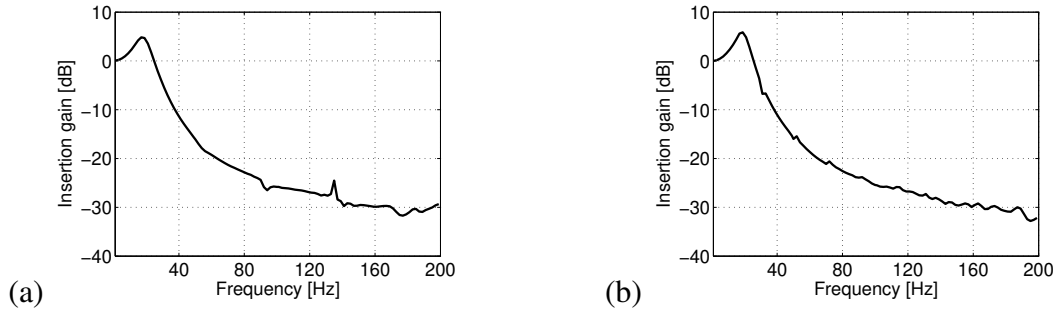

Figure 9: Insertion gain for 20 Hz floating slab at (a) 10 m and (b) 20 m above the tunnel.

5.3 Response to a moving harmonic load

Firstly, the response of the coupled track-tunnel-soil structure is presented for a moving harmonic load. The frequency content of the loading for this case is $\hat{g}(\omega) = 2\pi P \delta(\omega - \bar{\omega})$. The response due to a moving load on a periodic medium is given by equation (22). This equation now modifies to:

$$\begin{aligned} \hat{u}_i(\tilde{\mathbf{x}} + nL\mathbf{e}_y, \omega) &= \frac{P}{v} \exp\left[-i\left(\frac{\omega - \bar{\omega}}{v}\right)(nL - y_k)\right] \\ &\times \int_{-L/2}^{L/2} \exp\left[-i\left(\frac{\omega - \bar{\omega}}{v}\right)\tilde{y}'\right] \tilde{\hat{h}}_{zi}(\tilde{y}', \tilde{\mathbf{x}}, \kappa_0, \omega)\, \mathrm{d}\tilde{y}' \end{aligned} \tag{32}$$

where $\kappa_0 = (\omega - \bar{\omega})/v - 2m\pi/L$. A moving harmonic load with an excitation frequency $\bar{f} = 40$ Hz, a magnitude $P = 0.5$ N and a speed $v = 27$ m/s is considered on each rail.

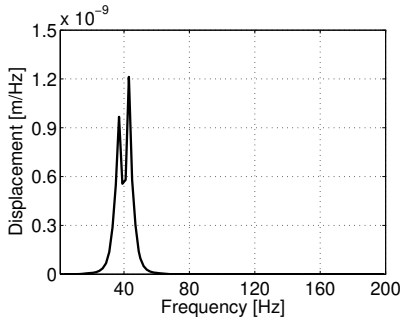

Figure 10: Vertical response at the driving point due to a moving harmonic load.

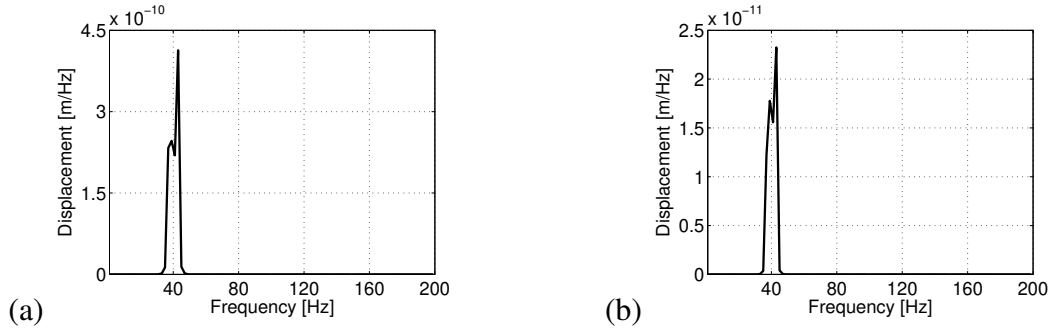

Figure 11: Vertical response at (a) the slab and (b) the tunnel invert due to a moving harmonic load.

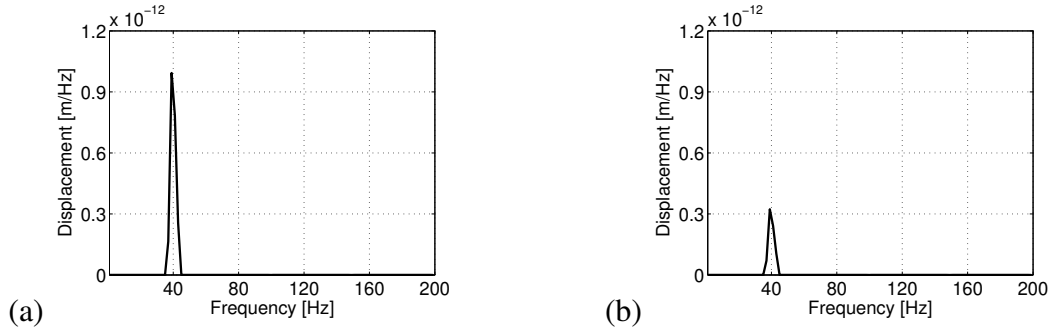

Figure 12: Vertical response at (a) 10 m and (b) 20 m above the tunnel due to a moving harmonic load.

Figures 10 and 11 show the vertical response of the rail, slab and tunnel invert for a moving harmonic load on the rails. There are two peaks in the response corresponding to the contribution of the bending waves in the track during the approaching and receding of the source. The frequency content is mainly situated in the range of the two peaks. This range of dominant frequencies increases, if the speed of the source increases and the Doppler effect is more clearly observed. Figure 12 shows the vertical response at 10 m and 20 m above the tunnel. The response has a distinct frequency content at the excitation frequency of 40 Hz and does not exhibit two peaks due to the Doppler effect. This is due to the fact that the speed of the source considered in the example is much less than the wave speeds in the soil.

5.4 Response due to rail roughness

Next, the excitation due to a more general moving load is considered. The wheel-rail interaction and vibrations are investigated using an artificial roughness profile, generated from the PSD curves. In this case, wheel-rail interaction is determined by the dynamic response of three components: the track, the wheel and the contact spring. The frequency response functions of the wheel and the track have a significant influence on the wheel-rail interaction as can be seen from equation (24). Typically, roughness levels are found to be high for long wavelengths (causing low frequency excitation) and low for short wavelengths (causing high frequency excitation) [22]. Figure 13a shows the PSD of the rail unevenness for different quality of rails. An intermediate curve (solid line) with reference value $\tilde{S}_{w/r}(k_{y0}) = 1.5 \times 10^{-8}\,\mathrm{m}^3/\mathrm{rad}$ between the two bounds of the PSD curves is chosen for generating the artificial roughness profile $u_{w/r}(y)$ as the superposition of cosine functions with random phase angles in the interval $[0, 2\pi]$ [23]. Figure 13b shows the magnitude of the roughness as a function of frequency for a speed $v = 27$ m/s.

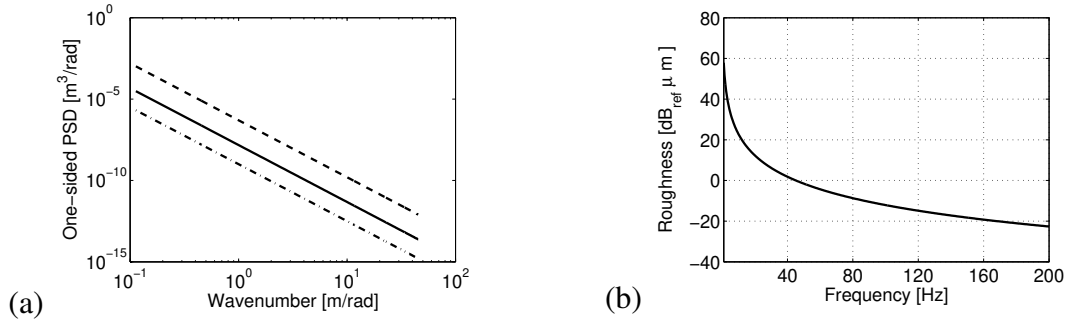

Figure 13: a) PSD curve of the unevenness of the rail (solid line) and its upper (dashed line) and lower (dashed-dotted line) bounds. (b) Magnitude of the roughness as a function of the frequency.

Mass parameters	Mass (kg)	
Wheel tread mass (M_1)	0	
Axle mass per wheel (M_2)	675	
Bogie mass per wheel (M_3)	2750	
Coach mass per wheel (M_4)	3300	
Spring parameters	Stiffness (N/m)	damping (Ns/m)
Resilient ring of the wheel (K_1^*)	0	0
Primary suspension (K_2, C_2)	2×10^6	5230
Secondary suspension (K_3, C_3)	1.4×10^5	2300

Table 1: Rolling stock parameters.

The properties of the track are the same as considered in the previous sections. Figure 14a shows the vertical point receptance of the rail calculated from the double beam model on an elastic foundation. Two peaks can be identified at the resonance frequencies, corresponding to the uncoupling of the track on the subgrade and the uncoupling of the rail on the rail pads, as explained before.

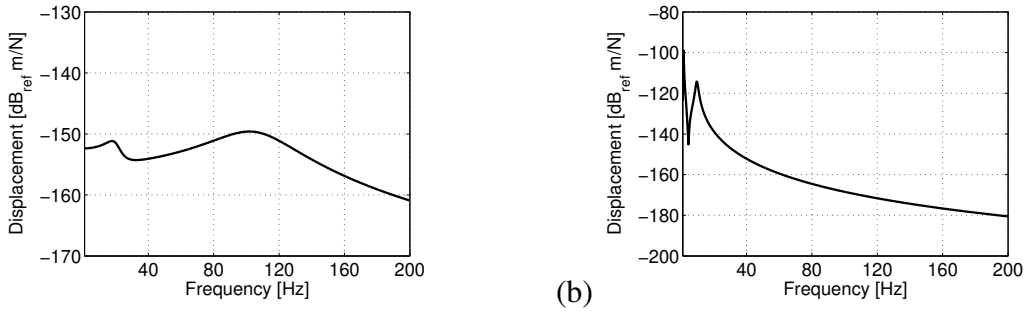

Figure 14: (a) Track receptance calculated from the double beam model on an elastic foundation. (b) Wheel receptance calculated from the rolling stock model.

Figure 14b shows the wheel receptance calculated according to the rolling stock parameters given in table 1. The first peak corresponds to the uncoupling of the coach on the bogie, which can be calculated as $1/(2\pi)\sqrt{K_3(1/M_3 + 1/M_4)} = 1.5$ Hz. The second resonance peak appears at $1/(2\pi)\sqrt{K_2(1/M_2 + 1/M_3)} = 9.6$ Hz, corresponding to the uncoupling of the bogie on the axle.

The contact receptance $\hat{C}^c = 7.97 \times 10^{-10}$ m/N is calculated from the linearized Hertzian theory [21] using the contact parameters; the wheel radius of curvature in the rolling direction $r_W = 0.46$ m and the rail radius in the transverse direction $r_R = 0.3$ m.

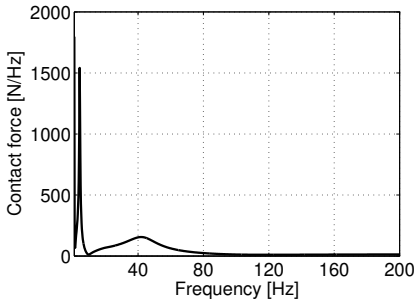

Figure 15: Contact force due to the wheel-rail interaction.

The contact force due to the wheel-rail interaction for the artificial roughness profile is calculated according to equation (24). Figure 15 shows the frequency content of the contact force applied on one rail. The first peak appears at $1/(2\pi)\sqrt{(K_2 + K_3)/M_3} = 4.4$ Hz, the anti-resonance of the primary suspension and secondary suspension on the bogie mass. The second peak appears at about 43 Hz, which corresponds to the wheel-track resonance. This can be evaluated considering the resonance of the unsprung mass of the rolling stock (wheel and axle) on the track stiffness. The static stiffness of the track $K_t = 4.1583 \times 10^7$ N/m is obtained by inverting the receptance of the rail at zero frequency. The total unsprung mass in this case is the mass of axle $M_2 = 675$ kg. The resonance frequency can approximately be calculated as $1/(2\pi)\sqrt{K_t/M_2} = 39.5$ Hz.

After the computation of the excitation force, equation (22) is used to compute the response due to moving load. It should be noted that the net excitation force is double the contact force shown in figure 15, as the model accounts for two rails with identical inputs. The rolling stock is

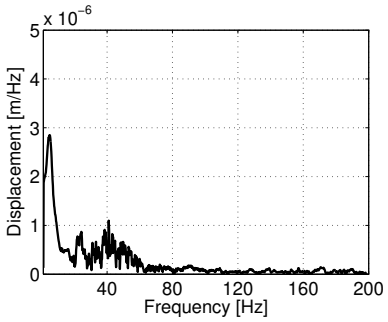

Figure 16: Vertical response at the rail due to a vehicle moving on a rough rail.

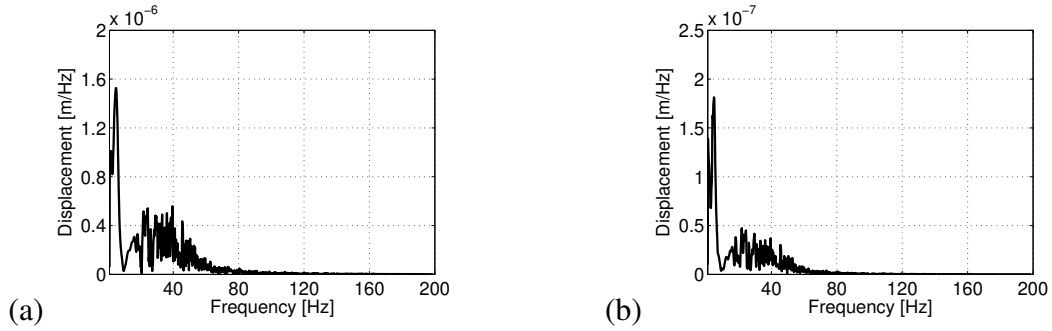

Figure 17: Vertical response at (a) the slab and (b) the tunnel invert due to a vehicle moving on a rough rail.

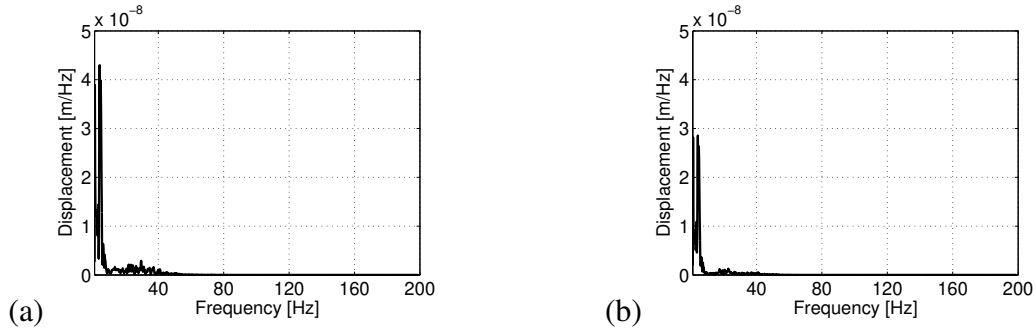

Figure 18: Vertical response at (a) 10 m and (b) 20 m above the tunnel due to a vehicle moving on a rough rail.

assumed to be moving at the speed of $v = 27$ m/s. Figures 16 and 17 show the vertical response at the rail, slab and tunnel invert due to this moving load. The maximum frequency content is around 4.4 Hz and 40 Hz, approximately at the position of the peaks in the contact force (figure 15). Figure 18 shows the vertical response at 10 m and 20 m above the tunnel. Response in the free field also exhibits peak at a first resonance frequency of the contact force. The frequency content is mainly situated between 0 and 45 Hz, with a shift towards the lower frequencies for an increasing distance from the source.

6 CONCLUSIONS

The main objective of the work presented in this paper is to prosper a better understanding of vibration from underground railways. A computational tool is presented which can be used to design the tracks in the tunnel and to assess the performance of vibration counter measures. Moreover, this tool can also be used to predict the free field vibrations due to a moving train.

The periodic finite element-boundary element formulation offers full modelling flexibility on a reference cell of the tunnel, which is an important advantage with respect to full three-dimensional or invariant models that are the two extremes of modelling complexities. In this paper, an invariant tunnel embedded in a homogeneous full space is modelled as a periodic structure.

The excitation due to rail unevenness and moving harmonic loads are considered. It is emphasized that the wheel/track interaction strongly depends on the dynamic response of the wheel, the rail and the contact springs. The track receptance is computed from the track model consisting of an infinite double beam on an elastic foundation, while the wheel receptance is obtained from the transfer matrix method applied on a rolling stock. The wheel-track interaction is first considered to estimate the excitation forces and then the track-tunnel-soil interaction problem is solved to compute the vibrations in the free field.

ACKNOWLEDGEMENTS

Shashank Gupta and Geert Degrande would like to thank IWT Vlaanderen, the Institute of the Promotion of Innovation by Science and Technology in Flanders. The results presented in this paper have been obtained within the frame of the SBO project IWT 03175 " Structural damage due to dynamic excitation: a multi-disciplinary approach", funded by IWT Vlaanderen. Their financial support is gratefully acknowledged.

REFERENCES

[1] M. Mohammadi and D.L. Karabalis. Dynamic 3-d soil-railway track interaction by BEM-FEM. *Earthquake Engineering and Structural Dynamics*, 24:1177–1193, 1995.

[2] O. von Estorff, M. Firuziaan, K. Friedrich, G. Pflanz, and G. Schmid. A three-dimensional FEM/BEM model for the investigation of railway tracks. In N. Chouw and G. Schmid, editors, *Proceedings of the International Workshop Wave 2000, Wave propagation, Moving load, Vibration reduction*, pages 157–172, Ruhr University, Germany, December 2000. A.A. Balkema, Rotterdam.

[3] K. Abe, D. Satou, T. Suzuki, and M. Furuta. Three-dimensional analysis of subway track vibrations due to running wheels. In N. Chouw and G. Schmid, editors, *Proceedings of the International Workshop Wave 2000, Wave propagation, Moving load, Vibration reduction*, pages 149–156, Ruhr University, Germany, December 2000. A.A. Balkema, Rotterdam.

[4] J. Dominguez. *Boundary Elements in Dynamics*. Co-published by Computational Mechanics Publications, Southampton, Boston and Elsevier Applied Science London, New York, 1993.

[5] A.A. Stamos and D.E. Beskos. Dynamic analysis of large 3-D underground structures by the BEM. *Earthquake Engineering and Structural Dynamics*, pages 1–18, 1995.

[6] A.A. Stamos and D.E. Beskos. 3-D seismic response analysis of long lined tunnels in half-space. *Soil Dynamics and Earthquake Engineering*, 15:111–118, 1996.

[7] D. Clouteau, M.L. Elhabre, and D. Aubry. Periodic BEM and FEM-BEM coupling: application to seismic behaviour of very long structures. *Computational Mechanics*, 25:567–577, 2000.

[8] R.J. Craig and M. Bampton. Coupling of substructures for dynamic analyses. *AIAA Journal*, 6(7):1313–1319, 1968.

[9] J.A. Forrest. *Modelling of ground vibration from underground railways*. PhD thesis, Department of Engineering, University of Cambridge, 1999.

[10] M.F.M. Hussein and H.E.M. Hunt. An insertion loss model for evaluating the performance of floating-slab track for underground railway tunnels. In *10th International Congress on Sound and Vibration*, Stockholm, Sweden, July 2003. CD-ROM.

[11] M.F.M. Hussein. *Vibration from underground railways*. PhD thesis, Department of Engineering, University of Cambridge, 2004.

[12] D. Clouteau, D. Aubry, M.L. Elhabre, and E. Savin. Periodic and stochastic BEM for large structures embedded in an elastic half-space. In *Mathematical Aspects of Boundary Element Methods*, pages 91–102. CRC Press, London, 1999.

[13] D. Clouteau, M. Arnst, T.M. Al-Hussaini, and G. Degrande. Free field vibrations due to dynamic loading on a tunnel embedded in a stratified medium. *Journal of Sound and Vibration*, 283(1–2):173–199, 2005.

[14] G. Degrande, D. Clouteau, R. Othman, M. Arnst, H. Chebli, R. Klein, P. Chatterjee, and B. Janssens. A numerical model for ground-borne vibrations from underground railway traffic based on a periodic finite element - boundary element formulation. *Journal of Sound and Vibration*, 2006. Special issue: Proceedings of the 8th International Workshop on Railway Noise. Accepted for publication.

[15] M.L. Elhabre. *Modélisation de l'interaction sismique sol-fluide-parois moulées suivant une approche périodique*. PhD thesis, Laboratoire de Mécanique des Sols, Structures et Matériaux, Ecole Centrale de Paris, 2000.

[16] G. Lombaert. *Development and experimental validation of a numerical model for the free field vibrations induced by road traffic*. PhD thesis, Department of Civil Engineering, K.U.Leuven, 2001.

[17] http://www.convurt.com, 2003.

[18] J. Charlier, P. Bouvet, and N. Vincent. Convurt Project. WP3: Development of excitation model. Report REF.450.003.RA.02.A, Vibratec, October 2002. CONVURT EC-Growth Project G3RD-CT-2000-00381.

[19] P.J. Remington. Wheel/rail rolling noise: what do we know? what don't we know? where do we go from here? 120(2):203–226, 1988.

[20] H. Braun and T. Hellenbroich. Messergebnisse von Strassenunebenheiten. *VDI Berichte*, 877:47–80, 1991.

[21] D.J. Thompson. Theory of generation of wheel/rail rolling noise. In V.V. Krylov, editor, *Noise and vibration from high-speed trains*, pages 3–26. Thomas Telford Publishing, London, 2001.

[22] P.J. Remington. Wheel and rail excitation from roughness. In V.V. Krylov, editor, *Noise and vibration from high-speed trains*, pages 27–64. Thomas Telford Publishing, London, 2001.

[23] C.Y. Yang. *Random vibration of structures*. John Wiley and Sons, London, 1986.